

# Numerical investigation on damping coefficient of the integral squeeze film damper<sup>①</sup>

LI Geng(李 耕)<sup>②</sup>, HE Lidong<sup>②</sup>, JIA Xingyun, ZHANG Yipeng, WANG Jian  
(Engineering Research Center of Chemical Safety Ministry of Education, Beijing University of Chemical Technology, Beijing 100029, P. R. China)

## Abstract

The elimination of rotor vibration is usually achieved by applying additional damping to the system. Squeeze film dampers are widely used in various aerospace and turbine equipments. The research is carried out on flow characteristics in the integral squeeze film dampers (ISFDs). The dynamic response to the operation condition is investigated through the computational fluid dynamics (CFD) model of ISFD. Due to the large pressure loss at the oil inlet, the oil film force only changes slightly with the increase of oil supply pressure, and the damping increases slightly. The vibration amplitude only affects the film force, but has no effect on the damping. The oil film force and damping show an upward tendency with the decrease of thickness of the end seal clearance.

**Key words:** integral squeeze film damper (ISFD), numerical method, oil film force, damping coefficient

## 0 Introduction

With the progress of technology and increasing production requirements, the rotation speed of rotating machinery is increasing, and the vibration problem of rotors is becoming more prominent. Applying damping elements in a rotating system can effectively dissipate vibration energy and reduce vibration.

Squeeze film dampers (SFDs) were proposed by Ref. [1]. Ref. [2] proposed an identification method suitable for nonlinear systems, and put forward a calculation model for the damping coefficient of oil film and the coefficient of inertial force. Through experiments, it was found that the damping coefficient and the coefficient of inertial force of SFD were basically consistent with model predictions.

In the 1960s, with the application of extrusion film damping, the dynamic characteristics of oil films were studied. Ref. [3] studied the stiffness of oil films and proposed the concept of extrusion films. Ref. [4] studied the influence of cavities on oil film pressure during the motion of oil film pressure. Ref. [5] studied the motion of the oil film-rotor system of the extruded oil film damper, calculated the oil film based on the short bearing assumption, and finally obtained a

calculation model of the oil film force.

Squeeze film dampers have been used in aerospace and turbo machinery<sup>[6-10]</sup>. In application, it is gradually found that the oil films of SFDs flow circumferentially, leading to a highly nonlinear problem of oil film force<sup>[11]</sup>.

The integral squeeze film damper (ISFD) was derived from a segmented SFD proposed by Ref. [12]. Ref. [13] carried out ISFD internal flow field research by using computational fluid dynamics (CFD) method. Refs[14,15] studied the vibration suppression of the ISFD rotor system and the unbalance vibration suppression of a G-type ISFD rotor system. Ref. [16] carried out ISFD vibration suppression research on gear transmission system. Ref. [17] studied the influence of end seal clearance on ISFD force coefficient.

## 1 CFD model of ISFD

The structure of an ISFD is shown in Fig. 1. The inner rim and outer rim constitute the ISFDs. The inner rim and outer rim are connected by 8 S-type elastomers, which are uniformly distributed in circumferential directions. The elastomers divide the oil film into eight discontinuous separate oil films. The ISFD journal does not rotate with the rotor, and the motion form

① Supported by the National Science and Technology Major Project (No. 2017- I V-0010-0047), China Postdoctoral Science Foundation Funded Project (No. 2020M670113) and Fundamental Research Funds for the Central Universities (No. JD2003).

② To whom correspondence should be addressed. E-mail: 1963he@163.com.

Received on Apr. 28, 2021

is only precession. Its equations of motion can be expressed as

$$X = e \cos(\Omega t) \quad (1)$$

$$Y = e \sin(\Omega t) \quad (2)$$

where  $X$  and  $Y$  are the precession displacement values of the ISFD journal in the  $X$  and  $Y$  directions,  $e$  is the rotor eccentricity,  $\Omega$  is the rotational angular velocity of the bearing, and  $t$  is time. Derivate Eqs(1) and (2), to obtain the speed values  $u$  and  $v$  of the journal in the  $X$  and  $Y$  directions, i. e. ,

$$u = -e\Omega \sin(\Omega t) \quad (3)$$

$$v = e\Omega \cos(\Omega t) \quad (4)$$

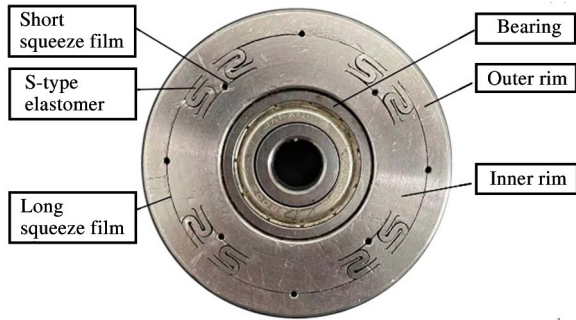


Fig. 1 Configuration of an ISFD with bearing

The ISFD possesses 8 segments (squeeze film lands). Long squeeze film lands are fed by oil supply nozzles, and the end seal clearance controls the outflow of the lube oil. The oil of short squeeze film lands comes from the end seal clearance. The oil enters the flow field from the oil supply nozzle and flows out from the end seal clearance. The oil flow path is shown in Fig. 2.

To reduce the calculation time, half of the model is used for calculation due to the symmetry of the model. The process arguments of the investigation ISFD are as follows. The thickness of the squeeze film is  $0.2 \times 10^{-3}$  m, the thickness of the end seal clearance is  $0.2 \times 10^{-3}$  m, the semidiameter of the oil supply nozzle is  $0.5 \times 10^{-3}$  m, the semidiameter of the outer squeeze film land is  $70 \times 10^{-3}$  m, the semidiameter of the inner squeeze film land is  $55 \times 10^{-3}$  m, the length of the ISFD is  $40 \times 10^{-3}$  m. The grade of the lube oil is ISO VG32 and the oil inlet temperature is 120 F (49 °C).

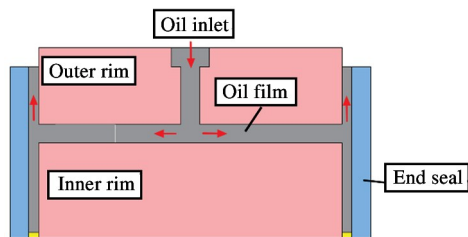


Fig. 2 Diagram of ISFD internal oil flow

Referring to standard, the density of the lube oil is  $870 \text{ kg/m}^3$  and the dynamic viscosity of the lube oil is  $0.019426 \text{ Pa} \cdot \text{s}$ .

The CFD model meshes are shown as Fig. 3. The element size of the CFD model is controlled to be smaller than  $0.3 \times 10^{-3}$  m. The aggregate number of cells in the grid is about 1 500 000.

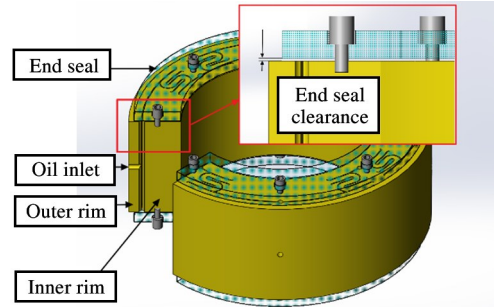


Fig. 3 ISFD with end seal cover

It is assumed that the oil is an incompressible Newtonian fluid, the coefficient of the oil viscosity is constant, there is no slip between the fluid and the rim external face, and gravity is not considered in the CFD model. The cavitation phenomenon is not considered in the calculation of hydraulic pressure.

The squeeze film Reynolds number indicates the inertia of fluid and turbulence effects in ISFDs. The Reynolds equation of the compressed oil film fluid is

$$Re = \frac{\rho \Omega c^2}{\mu} \quad (5)$$

where  $\rho$  is the density of the oil,  $\mu$  is the viscosity of the oil,  $\Omega$  is the precession angular velocity of the bearing, and  $c$  is the thickness of the squeeze film land. The synchronous circular rotation frequency is 50 Hz and the semidiameter of the rotational track is  $6 \times 10^{-6}$  m.

According to Eq. (5), the Reynolds number is equal to 0.188 and the Reynolds number of turbulence is  $Re \approx 2000$ . The critical Reynolds number is much larger than the Reynolds number calculated under this condition. Therefore, the viscous model is set to laminar in Fluent software.

The oil flows in from the oil supply nozzle, and flows out of the end seal clearance. The inner rim moves with the bearing, and there is no relative rotation between the inner rim and the outer rim. According to the working principle of ISFD, the boundary conditions (Fig. 4) are defined, the oil supply nozzles are set to pressure inlet, the end seal clearances are set to pressure outlet, and other faces are set to wall.

The inner walls of squeeze film lands are forced to move, so dynamic mesh is set at the inner walls of squeeze film lands. The moving speed of the inner

walls of squeeze film lands is the same as the circular whirling of the journal. The outer walls of the squeeze film lands are static.

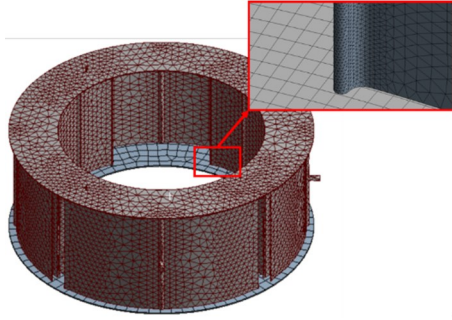


Fig. 4 The meshes of the ISFD

Dynamic mesh model can be used to simulate the flow field since the motion of the boundary shape changes over time. Boundary movement form can be a pre-defined movement, which can be specified before calculating the speed or angular velocity, the boundary of sport will be decided by the calculation result of the previous step. Mesh update process by the Fluent software according to each boundary changed automatically. When using dynamic mesh model, it is necessary to first define the initial mesh, boundary movement way and specify the regions that participate in the motion. The model boundary function can be used or user defined function (UDF) can define border movements.

For any  $V$ , the integral conservation equation of general scalar  $\Phi$  is

$$\begin{aligned} \frac{d}{dt} \int_V \rho \Phi dV + \int_{\partial V} \rho \Phi (\vec{u} - \vec{u}_g) \cdot d\vec{A} \\ = \int_{\partial V} \Gamma \nabla \Phi (\vec{u} - \vec{u}_g) \cdot d\vec{A} + \int_V S_\phi dV \end{aligned} \quad (6)$$

where  $V$  is the control volume,  $\vec{u}$  is the flow velocity vector,  $\vec{u}_g$  is the mesh velocity of the moving mesh,  $\Gamma$  is the diffusion coefficient,  $S_\phi$  is the source term of  $\Phi$ ,  $\partial V$  is the boundary of the control volume  $V$ .

By using a first-order backward difference formula, the time derivative term in Eq. (6) can be written as Eq. (7). In Eq. (7),  $n + 1$  and  $n$  represent different time level. The  $(n + 1)$ th time level volume  $V^{n+1}$  is computed from Eq. (8).

$$\frac{d}{dt} \int_V \rho \Phi dV = \frac{(\rho \Phi V)^{n+1} - (\rho \Phi V)^n}{\Delta t} \quad (7)$$

$$V^{n+1} = V^n + \frac{dV}{dt} \Delta t \quad (8)$$

where  $dV/dt$  is the volume time derivative of the control volume  $V$ . In order to satisfy the mesh conservation law, the volume time derivative of the control volume is computed from Eq. (9), where  $n_f$  is the number of the

faces on the control volume  $V$ . The dot product  $\vec{u}_{g,j} \cdot \vec{A}_j$  on each control volume face is calculated as

$$\frac{dV}{dt} = \int_{\partial V} \vec{u}_g \cdot d\vec{A} = \sum_j^{n_f} \vec{u}_{g,j} \cdot \vec{A}_j \quad (9)$$

$$\vec{u}_{g,j} \cdot \vec{A}_j = \frac{\delta V_j}{\Delta t} \quad (10)$$

## 2 Results of the computational simulations

In order to study the influence of operation condition on oil film force, a single variable numerical simulation is carried out. The variation in forces under different conditions during one period is studied. It is hereby explained that as the model used in the calculation is a scaled-down model and the procession amplitude is set to be small in order to prevent the overlap of the model boundary which will cause negative mesh, the calculation force is small.

### 2.1 Influence of the thickness of the end seal clearance on oil film force

Oil flows out from the end seal clearance. The thickness of the end seal clearance determines how easy it is for oil to flow out. In other words, the thickness of the end seal clearance plays an important role in oil flow, and affects the oil film forces.

Numerical simulations for different thickness of the end seal clearance are carried out. Boundary conditions: pressure inlet boundary is 0.10 MPa, pressure outlet boundary is 0, the eddy amplitude is 6  $\mu\text{m}$ . The pressure distributions for four values of the thickness of the end seal clearance are depicted in Fig. 5. As seen from Fig. 5, it is clear that total pressure increases with the decreases in the thickness of end seal. And the oil film force increases. The pressure distribution is more uniform throughout the ISFD. Fluid flowing is more difficult with thinner end seal clearance.

The velocity magnitude for four values of the thickness of the end seal clearance are depicted in Fig. 6. The velocity magnitude decreases with the decreases in the thickness of end seal. The maximum velocity magnitude is 16.01 m/s for 0.25 mm of the thickness of the end seal clearance in ISFD, while the maximum velocity magnitude is 7.156 m/s for 0.1 mm of the thickness of the end seal clearance in ISFD. The thin end seal clearance severely impedes the flow of oil.

The time history of the short oil film force in the radial and tangential directions for four values of the thickness of the end seal clearance is depicted in Fig. 7.

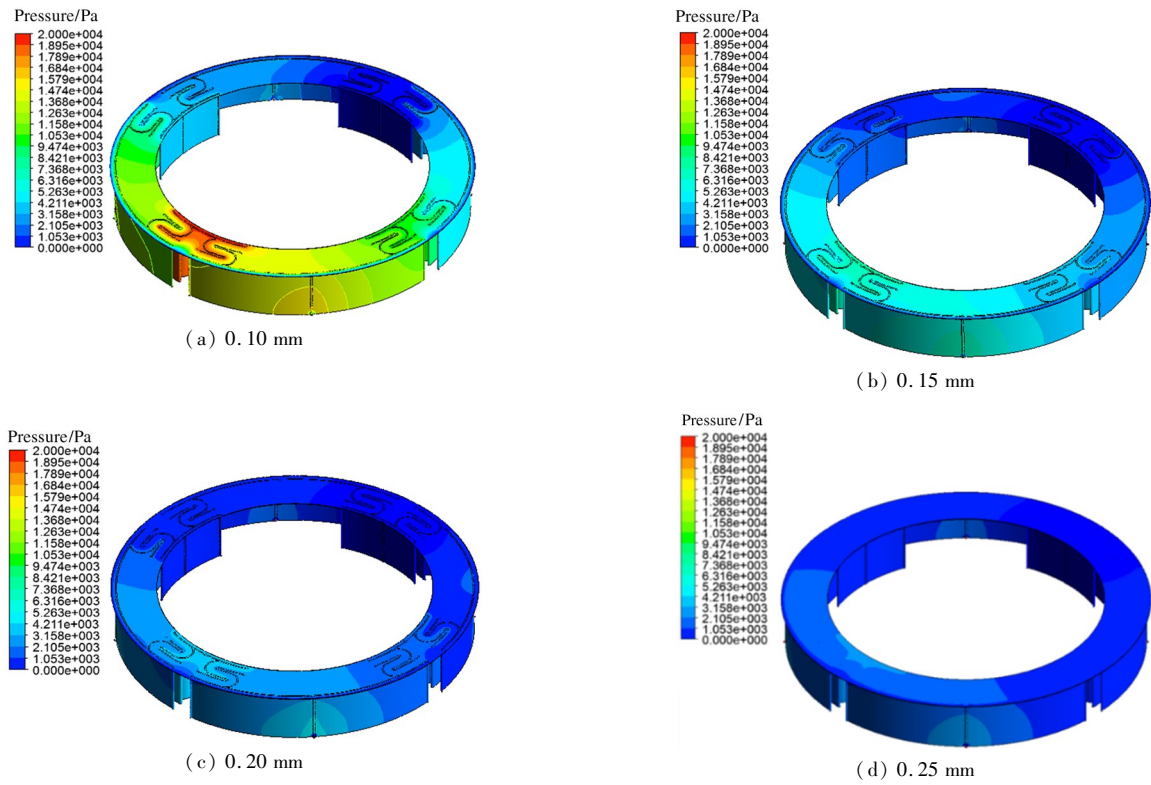


**Fig. 5** Pressure distribution under different thickness of the end seal clearance

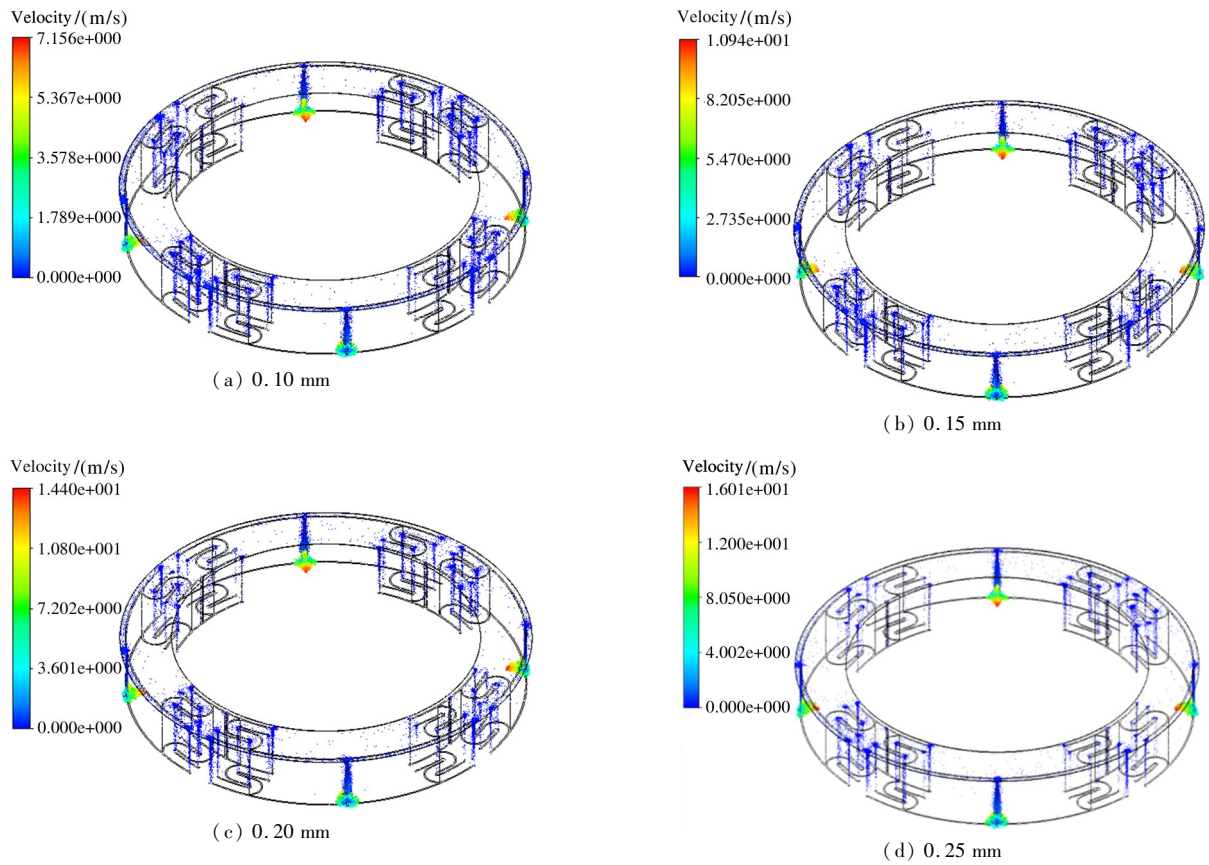


**Fig. 6** Effect of thickness of the end seal clearance on velocity distribution in ISFD

As can be seen from Fig. 7, the magnitude of oil film force changes in X direction and Y direction in-

creases with the end seal clearance getting thinner. The magnitude of oil film force changes in X and Y di-

rections are 147.38 N and 146.39 N when the end seal clearance is 0.1 mm. And the magnitudes are 21.70 N and 21.23 N when the end seal clearance is 0.25 mm. This is because as the end seal thickness becomes thin-

ner, the flow of oil becomes more difficult, the obstruction increases, and the force on the oil film also increases.

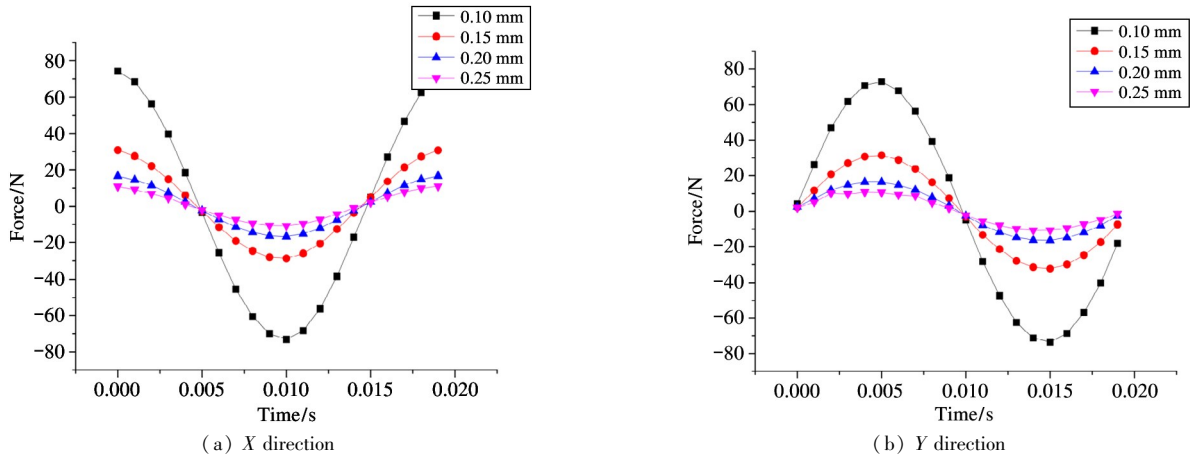


Fig. 7 Time history of oil film force in X and Y directions under different end seal clearances

### 2.2 Influence of vibration amplitude on oil film force

The whirl of the rotor is transmitted to the bearing, which in turn is transmitted to ISFD. In general, the amplitude of rotor whirl is not fixed. In order to study the influence of rotor vibration amplitude on oil film force, different vibration amplitudes are employed.

The simulations for four values of the vibration

amplitude (6  $\mu\text{m}$ , 8  $\mu\text{m}$ , 10  $\mu\text{m}$  and 12  $\mu\text{m}$ ) are carried out. Boundary conditions are that the pressure inlet boundary is 0.10 MPa and the pressure outlet boundary is 0. The pressure distribution in ISFD under different vibration amplitude is depicted in Fig. 8. With the increase in rotor vibration amplitudes, the pressure distributions of ISFD for four values of vibration amplitudes are similar.

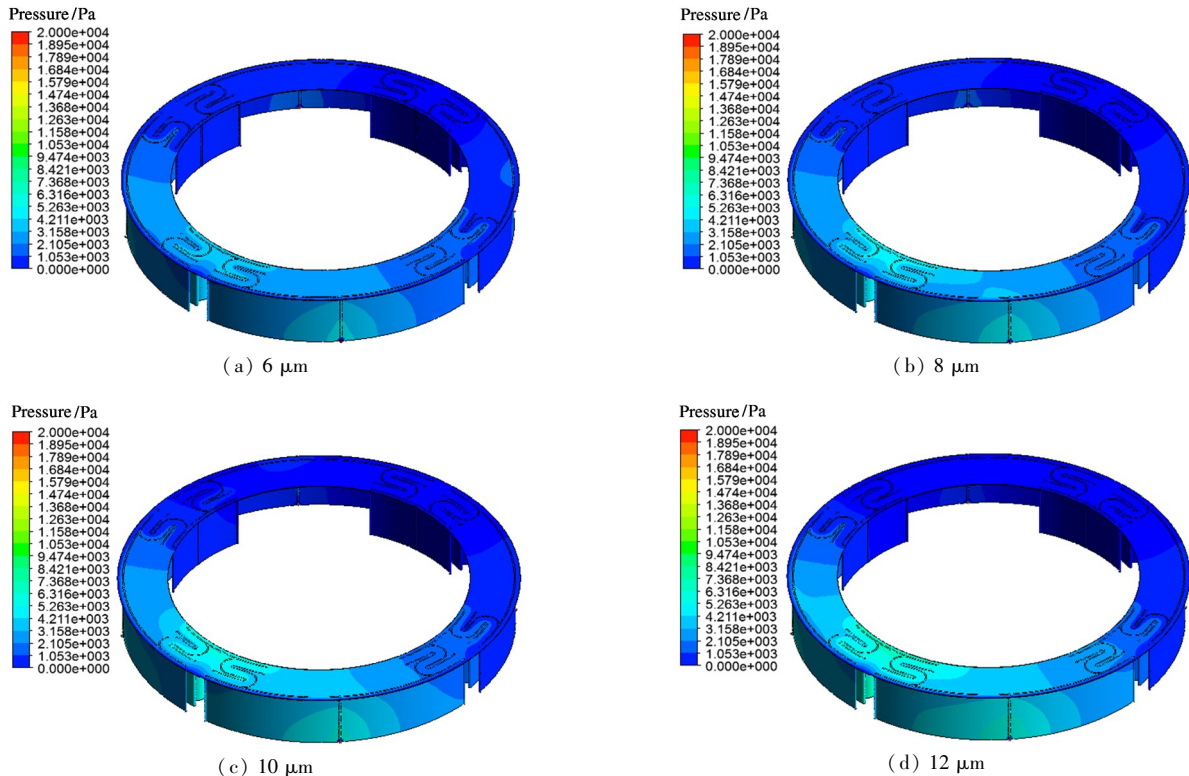


Fig. 8 Pressure distributions under different vibration amplitudes

The velocity magnitude in ISFD under different vibration amplitudes is depicted in Fig. 9. The maximum velocity magnitudes for the 4 types of vibration amplitudes are in the range of 14.40 – 14.48 m/s, therefore, the change of the vibration amplitude is not the

reason of the increase in the internal flow velocity of ISFD. The time history of oil film force in X direction is depicted in Fig. 10(a) and the time history of oil film force in Y direction is depicted in Fig. 10(b).

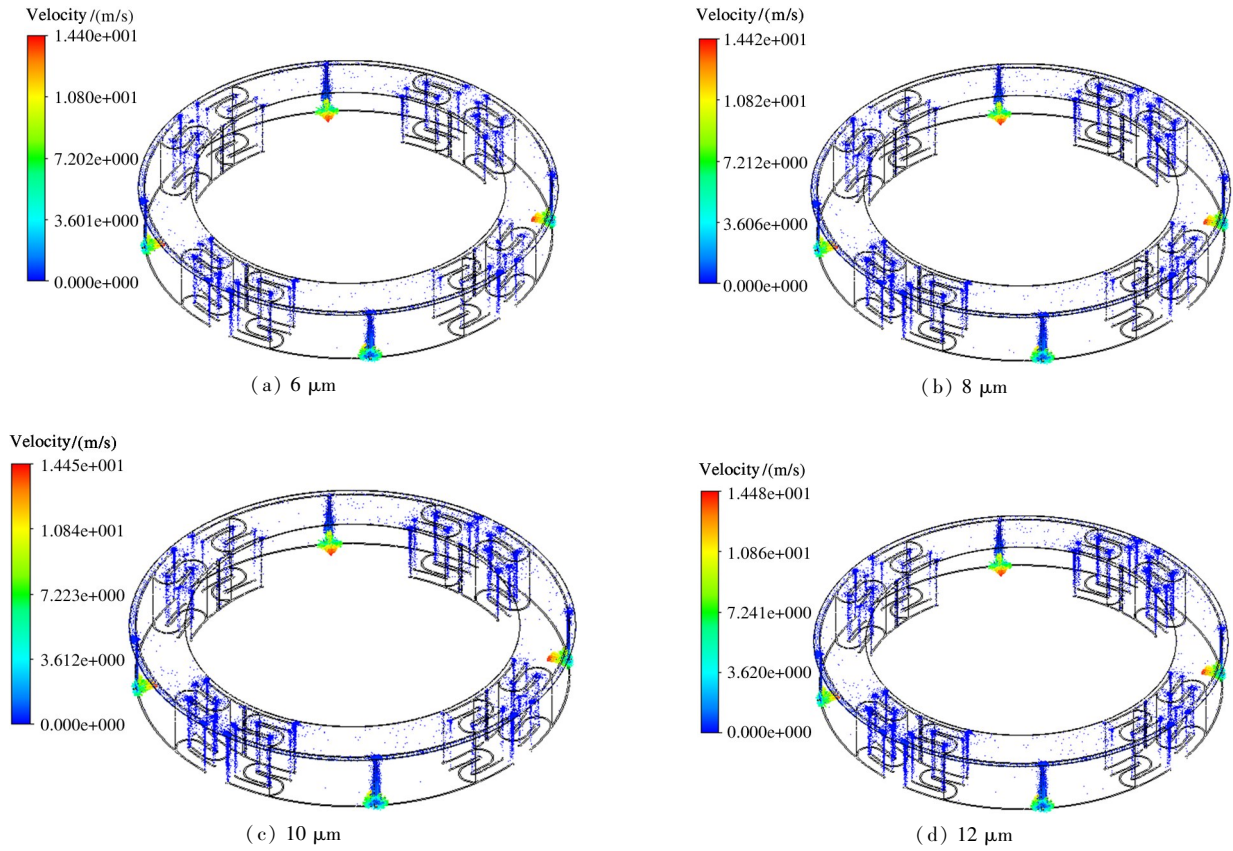


Fig. 9 Velocity under different vibration amplitudes

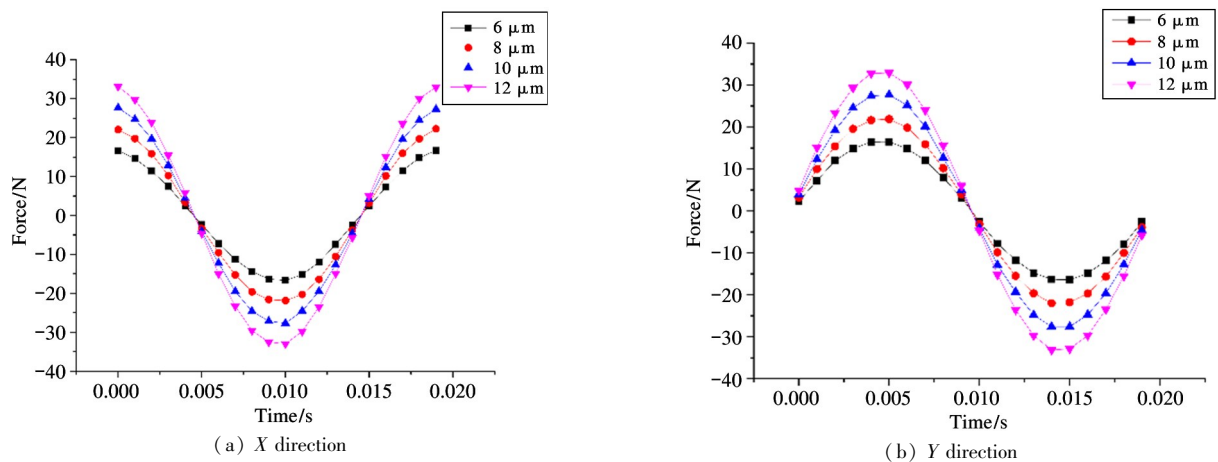


Fig. 10 Time history of oil film force in X and Y directions under different vibration amplitudes

It can be seen from Fig. 10(a) and 10(b) that with the increase of vibration amplitude, the fluctuation of the oil film forces in both X direction and Y direction increases. When the vibration amplitude is 6 μm, the magnitude of oil film force changes in X and Y direc-

tion are 33.42 N and 32.90 N. When the vibration amplitude is 12 μm, the changes of the magnitude of oil film force in X and Y directions are 66.11 N and 66.06 N.

### 2.3 Influence of oil supply pressure on oil film force

Numerical simulations are performed with the values of oil supply pressure changes (0.08 MPa, 0.10 MPa, 0.12 MPa and 0.14 MPa). The pressure distribution is depicted in Fig. 11. As seen from Fig. 11, the pressure of the squeeze film on ISFD is affected by rotor whirl, and the distribution difference occurs. The pressure in

the squeezed position is bigger than that in the unsqueezed position. The pressure distribution between adjacent oil films is approximately continuous, ensuring the continuity of the ISFD's oil film forces in the circumferential region. However, with the increase of oil supply pressure, the force on the oil film does not increase significantly. This is due to the significant loss of oil pressure from the inlet to the oil film, resulting in a similar pressure distribution across the oil film.

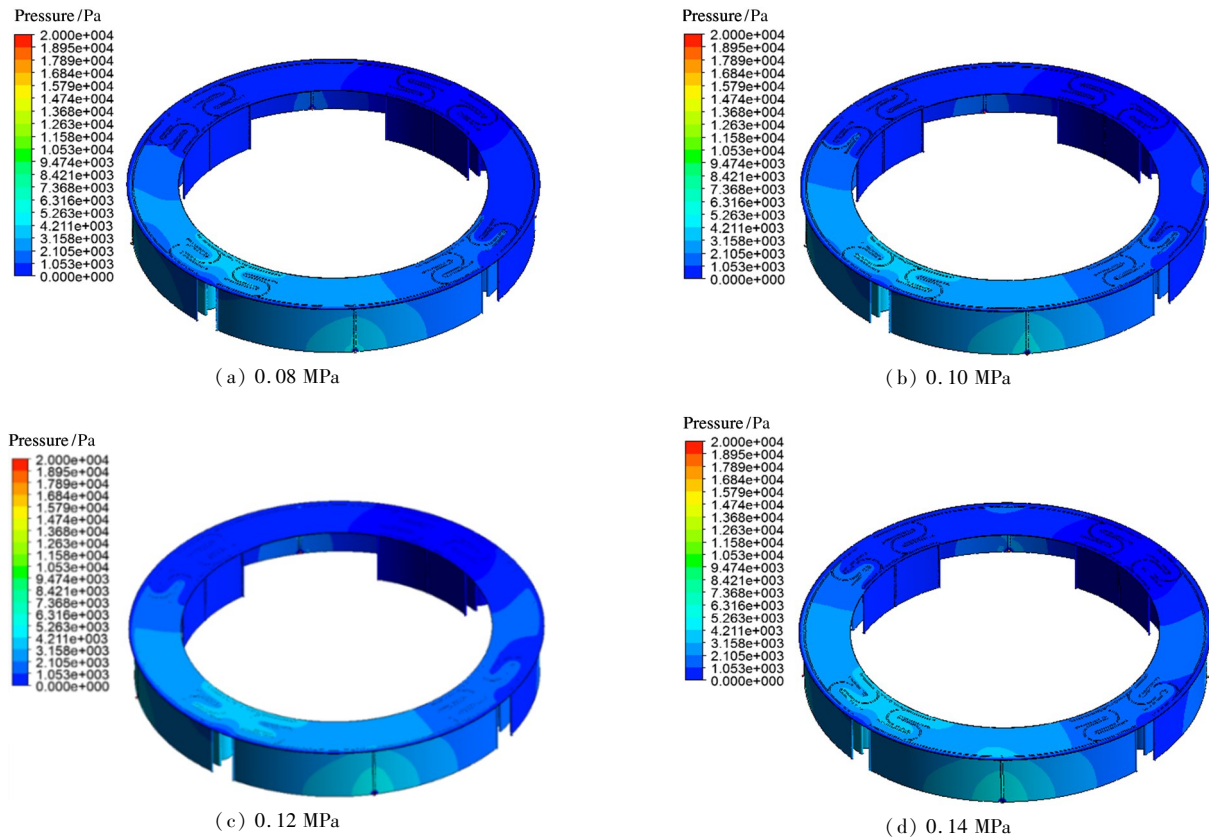


Fig. 11 Pressure distribution under different oil supply pressures

The velocity is depicted in Fig. 12. The largest velocity magnitude increases from 12.85 m/s to 17.12 m/s as the oil supply pressure increases from 0.08 MPa to 0.14 MPa. It is obvious that the increase in velocity magnitude is caused by the enhancement of oil supply pressure. To analyze the changes in oil film force, the long squeeze film land and short squeeze film land are taken for pressure integration to obtain the oil film force. Transient analysis is used to compute the time dependence of the oil film force. The time history of oil film force in  $X$  direction is depicted in Fig. 13(a) and the time history of oil film force in  $Y$  direction is depicted in Fig. 13(b).

It can be seen from Fig. 13 that the oil film force changes periodically with the rotor whirl, and the change period is the same as that of the rotor whirl.

The force phase difference between  $X$  direction and  $Y$  direction is  $\pi/2$ . Since the pressure distribution on the oil film is similar, there is no significant difference in the oil film forces under each oil supply pressure in  $X$  and  $Y$  directions.

### 3 Damping coefficient calculation

The study of oil film force of squeeze film damper is the basis of analysis and design of squeeze film damper. From the mathematical point of view, the core problem of dynamic characteristics of squeeze oil film is to solve the pressure distribution law of oil film in the Reynolds equation. The transient Reynolds equation of the squeeze film damper is

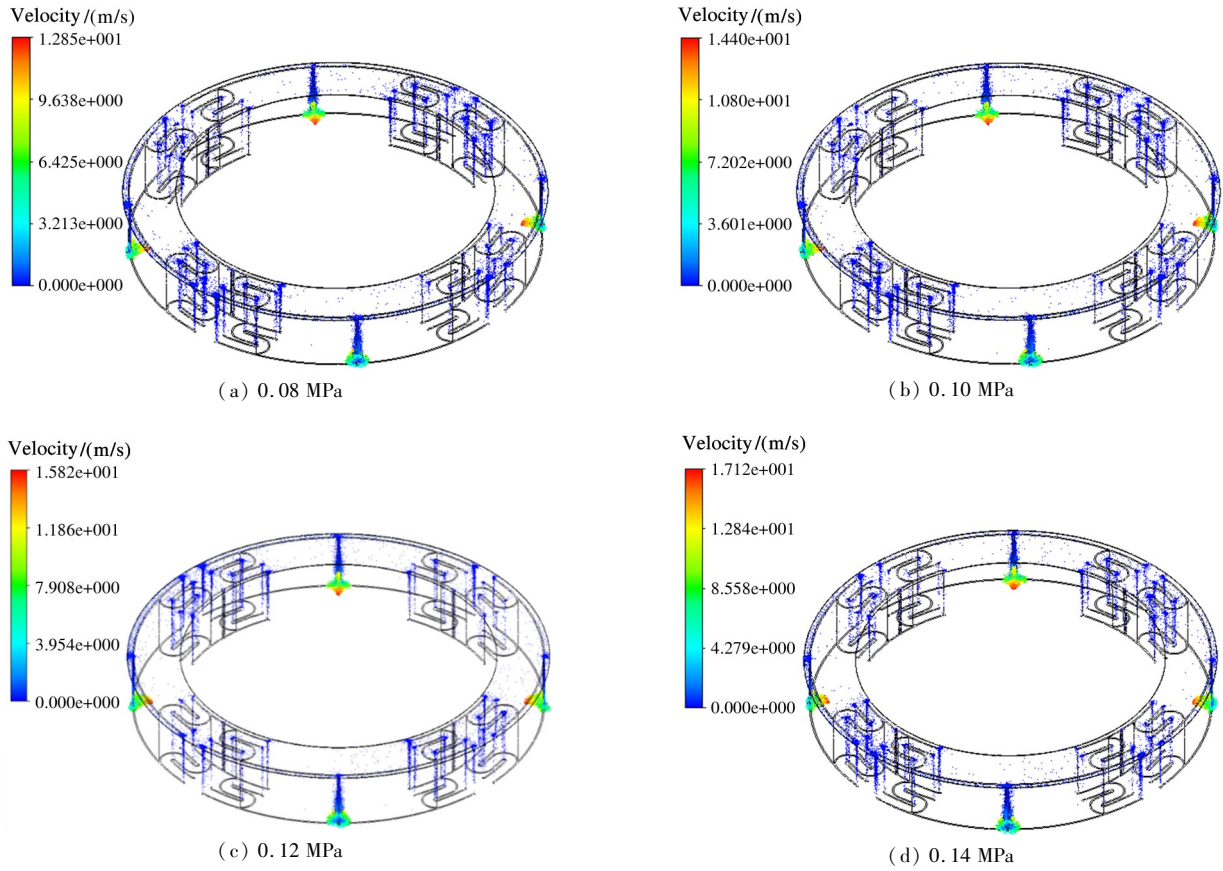


Fig. 12 Velocity under different oil supply pressures

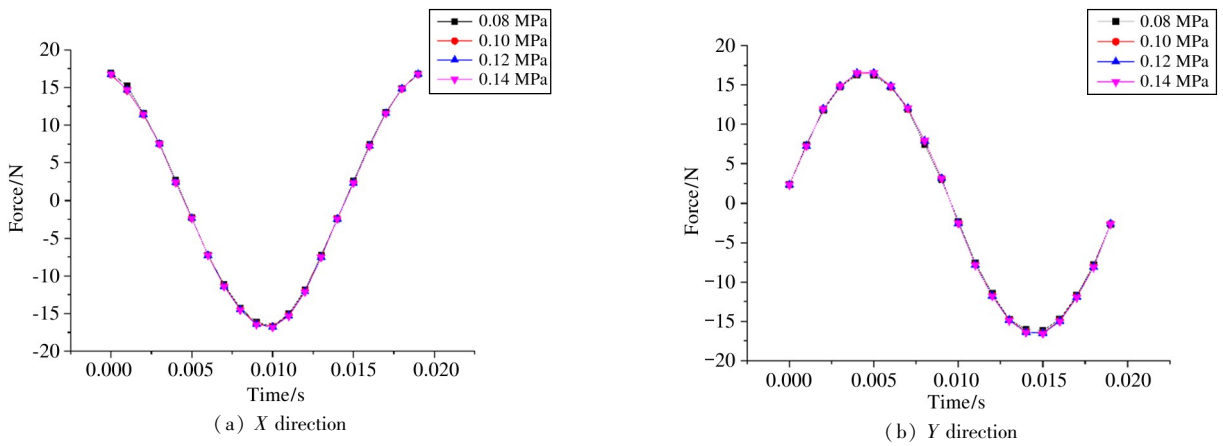


Fig. 13 Time history of oil film force in X and Y directions under different oil supply pressures

$$\frac{\partial}{\partial \theta} \left[ (1 + \varepsilon \cos \theta)^3 \frac{\partial P}{\partial \theta} \right] + R^2 \frac{\partial}{\partial z} \left[ (1 + \varepsilon \cos \theta)^3 \frac{\partial P}{\partial z} \right] = \frac{12\mu R^2}{c^2} (\varepsilon \Omega \sin \theta + \varepsilon \cos \theta) \quad (11)$$

The Reynolds equation is binary quadratic inhomogeneous nonlinear partial differential equation with variable coefficients, which is difficult to solve. Before the computer emerging, in order to obtain the distribution of oil film pressure, people had made a lot of assumptions and simplifications on the Reynolds equation. The short bearing hypothesis and long bearing hypothesis are widely used.

When there is no end sealing device at both ends of the damper, and the pressure at both ends of the damper is the same as the external pressure and the slender-diameter ratio is less than 0.25, the hypothesis of short bearing is in good agreement with the actual results. The change of pressure gradient along the circumference is much smaller than the change of pressure in

the axial direction, i. e.,  $\frac{\partial P}{\partial z} \gg \frac{\partial P}{\partial \theta}$ . In this case,  $\frac{\partial P}{\partial \theta}$  can be considered to be equal to 0. In other words, the approximate formula of short bearing hypothesis can be obtained.

$$\frac{\partial}{\partial z} \left[ (1 + \varepsilon \cos \theta)^3 \frac{\partial P}{\partial z} \right] = \frac{12\mu}{c^2} (\varepsilon \Omega \sin \theta + \varepsilon \cos \theta) \quad (12)$$

According to the pressure distribution of the extruded oil film damper, eight dynamic characteristic coefficients can be derived under the condition of semi-oil film and full oil film. Under semi-oil film condition, the eight dynamic characteristic coefficients of the short bearing squeeze film damper of the concentric precession are as Eq. (13). Similarly, under the condition of full oil film, the eight dynamic characteristic parameters of concentric precession short bearing squeeze film damper are expressed as Eq. (14).

$$\begin{cases} K_{rr} = \frac{\mu RL^3}{c^3} \cdot \frac{4\Omega \varepsilon_0 (1 + \varepsilon_0^2)}{(1 - \varepsilon_0^2)^3} & K_{rt} = \frac{\mu RL^3}{c^3} \cdot \frac{\pi \Omega}{2(1 - \varepsilon_0^2)^{3/2}} \\ K_{rr} = \frac{\mu RL^3}{c^3} \cdot \frac{\pi \Omega (1 + 2\varepsilon_0^2)}{(1 - \varepsilon_0^2)^{5/2}} & K_{ru} = \frac{\mu RL^3}{c^3} \cdot \frac{2\Omega \varepsilon_0}{(1 - \varepsilon_0^2)^2} \\ C_{rr} = \frac{\mu RL^3}{c^3} \cdot \frac{\pi (1 + 2\varepsilon_0^2)}{2(1 - \varepsilon_0^2)^{5/2}} & C_{rt} = \frac{\mu RL^3}{c^3} \cdot \frac{2\varepsilon_0}{(1 - \varepsilon_0^2)^2} \\ C_{rr} = \frac{\mu RL^3}{c^3} \cdot \frac{2\varepsilon_0}{(1 - \varepsilon_0^2)^2} & C_{ru} = \frac{\mu RL^3}{c^3} \cdot \frac{\pi}{2(1 - \varepsilon_0^2)^{3/2}} \end{cases} \quad (13)$$

$$\begin{cases} K_{rr} = 0 & K_{rt} = \frac{\mu RL^3}{c^3} \cdot \frac{\pi \Omega}{2(1 - \varepsilon_0^2)^{3/2}} \\ K_{rr} = \frac{\mu RL^3}{c^3} \cdot \frac{\pi \Omega (1 + 2\varepsilon_0^2)}{(1 - \varepsilon_0^2)^{3/2}} & K_{ru} = 0 \\ C_{rr} = \frac{\mu RL^3}{c^3} \cdot \frac{\pi (1 + 2\varepsilon_0^2)}{2(1 - \varepsilon_0^2)^{5/2}} & C_{rt} = 0 \\ C_{rr} = 0 & C_{ru} = \frac{\mu RL^3}{c^3} \cdot \frac{\pi}{(1 - \varepsilon_0^2)^{3/2}} \end{cases} \quad (14)$$

In the long bearing hypothesis, the effective length and diameter ratio of the damper tends to infinity, and when there is no seal at both ends of the damper, the pressure gradient along the axial direction in the damper is small, i. e.,  $\frac{\partial P}{\partial z} \ll \frac{\partial P}{\partial \theta}$ . At this point,  $\frac{\partial P}{\partial z}$  can be approximately considered to be equal to 0, and the Reynolds equation under the long bearing hypothesis is as follows.

$$\frac{\partial}{\partial \theta} \left[ (1 + \varepsilon \cos \theta)^3 \frac{\partial P}{\partial \theta} \right] = \frac{12\mu R^2}{c^2} (\varepsilon \Omega \sin \theta + \varepsilon \cos \theta) \quad (15)$$

When the mass center of the journal precession is steadily around the center of the shaft, and the trajectory of the shaft center is a standard circle, the eight

dynamic parameters of the extrusion film damper can be simplified to two equivalent damping parameters. For semi-oil film condition, they are shown in Eq. (16). And under full oil film condition, they are shown as Eq. (17).

$$\begin{cases} K_c = 6\mu L \left(\frac{R}{c}\right)^3 \frac{4\Omega \varepsilon}{(2 + \varepsilon^2)(1 - \varepsilon^2)} \\ C_c = 12\mu L \left(\frac{R}{c}\right)^3 \frac{\pi}{(2 + \varepsilon^2)(1 - \varepsilon^2)^{0.5}} \end{cases} \quad (16)$$

$$\begin{cases} K_c = 0 \\ C_c = 24\mu L \left(\frac{R}{c}\right)^3 \frac{\pi}{(2 + \varepsilon^2)(1 - \varepsilon^2)^{0.5}} \end{cases} \quad (17)$$

Both short bearing hypothesis and long bearing hypothesis have their own scope of application, and their accuracy and scope of application are often inversely proportional. Both short bearing hypothesis and long bearing hypothesis do not apply to ISFDs. As seen from Fig. 13, it is obvious that the thickness of end seal clearance has big effect on ISFD's pressure distribution. This means that the end seal clearance will affect stiffness and damping, while there is no end seal clearance in Eqs(13), (14), (16) and (17). So another formula for calculating damping coefficient is proposed. The oil film's equivalent damping coefficient is

$$C_0 = -\frac{F_t}{e\Omega} \quad (18)$$

where  $F_t$  is the damping force component of oil film force, which is in the opposite direction of journal precession,  $e$  is the rotor eccentricity, and  $\Omega$  is the rotational angular velocity.  $F_t$  can be solved from the following formulas.

$$F_r = F_x \cos(\omega t) - F_y \sin(\omega t) \quad (19)$$

$$F_t = F_x \sin(\omega t) + F_y \cos(\omega t) \quad (20)$$

Numerical simulation has been performed to verify the accuracy of the Eq. (18). CFD model of ISFD fluid domain was constructed by referring to Ref. [18].

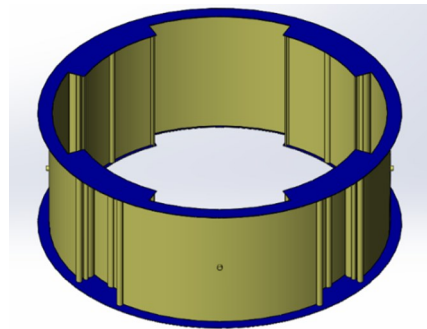


**Fig. 14** CFD model of ISFD fluid domain referring to Ref. [18]

The operation condition parameters are the same as those in Ref. [18]. The oil supply pressure is 0.14 MPa,

and vibration amplitude is  $6.35 \mu\text{m}$ , and the lubricant is ISO VG32 and the temperature is  $49 \text{ }^\circ\text{C}$ . Numerical simulation results are substituted into Eq. (18), and the average damping coefficient of the ISFD under this operation condition is  $33\,886.16 \text{ N}\cdot\text{s}/\text{m}$ . Damping coefficient in Ref. [18] under this operation condition is  $37\,000 \text{ N}\cdot\text{s}/\text{m}$ . The similarity of the calculated results is  $91.58\%$ . In another operation condition, the damping coefficient is  $138\,418 \text{ N}\cdot\text{s}/\text{m}$ , and the damping coefficient in Ref. [18] is  $152\,000 \text{ N}\cdot\text{s}/\text{m}$ . The similarity of the calculated results is  $91.06\%$ . Some subtle structural differences in the model and slight differences in lubricant viscosity limit the higher similarity of the two damping coefficients calculated. The similarity of more than  $90\%$  proves the reliability of Eq. (18).

### 3.1 Influence of the thickness of the end seal clearance on damping coefficient

The damping changes four times in a period of journal precession, and the damping is periodic, because the oil film is arranged symmetrically in four groups in ISFD. Increasing the oil supply pressure is an effective way to improve the ISFD damping.

The damping coefficients of the ISFD under different thickness of the end seal clearance are depicted in Fig. 15. The damping coefficient is  $5620.09 \text{ N}\cdot\text{s}/\text{m}$  when the end seal clearance is  $0.25 \text{ mm}$ . When the end seal clearance is reduced to  $0.10 \text{ mm}$ , the damping coefficient increases to  $39\,226.8 \text{ N}\cdot\text{s}/\text{m}$ . Thin end seal clearance causes large damping. The damping coefficients tend to increase with the decrease of end seal clearance thickness. The end seal clearance becomes thinner, the oil is difficult to flow, and the oil film hinders the precession.

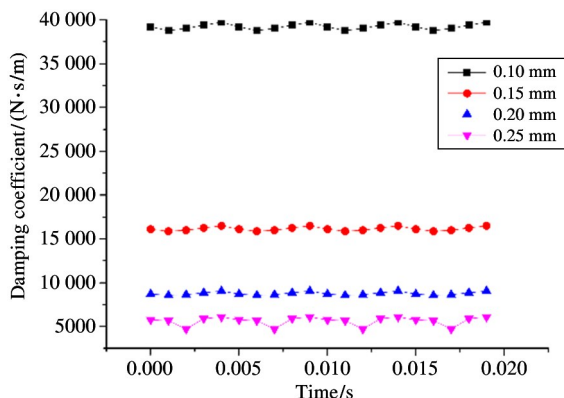


Fig. 15 Damping coefficients under different end seal clearances

### 3.2 Influence of the vibration amplitude on damping coefficient

The oil film forces calculated in subsection 2.2

are processed and substituted into Eq. (18). The calculated results are shown in Fig. 16.

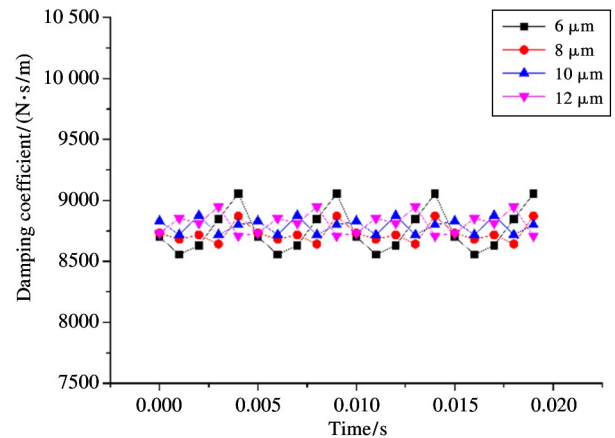


Fig. 16 Damping coefficients under different vibration amplitudes

As can be seen from Fig. 16, the damping provided by ISFD does not increase with the increase of vibration amplitude. The damping coefficient is  $8758.24 \text{ N}\cdot\text{s}/\text{m}$  when the vibration amplitude is  $6 \mu\text{m}$ . And the damping coefficient rises to  $8811.16 \text{ N}\cdot\text{s}/\text{m}$  when the vibration amplitude is  $12 \mu\text{m}$ . Although the oil film force increased, the equivalent damping is inversely proportional to the vibration amplitude, and the equivalent damping is almost constant under the interaction of these 2 factors.

### 3.3 Influence of the oil supply pressure on damping coefficient

The oil film forces calculated in subsection 2.3 are processed and substituted into Eq. (18). The damping coefficients of ISFD under different oil supply pressures are shown in Fig. 17.

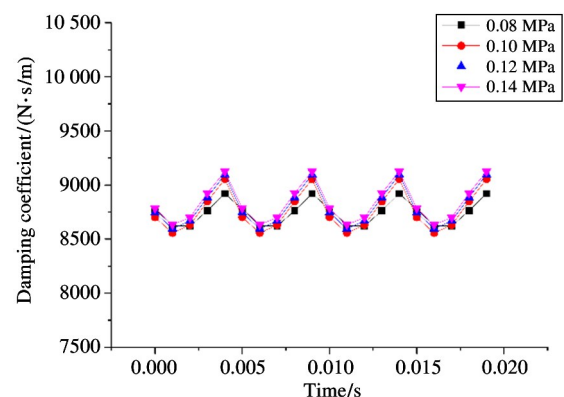


Fig. 17 Damping coefficients under different oil supply pressures

As shown in Fig. 17, the damping of ISFD is slightly increased with the increase of oil supply pressure. This is due to the pressure loss at inlet. When the oil supply pressure is  $0.08 \text{ MPa}$ , the average damping

is  $8740 \text{ N} \cdot \text{s/m}$ . When the oil supply pressure increases to  $0.12 \text{ MPa}$ , the average damping is  $8798 \text{ N} \cdot \text{s/m}$ .

#### 4 Conclusions

The influences of oil thickness of the end seal clearance, vibration amplitude, and oil supply pressure on the ISFD oil film force and damping are presented by numerical method in this research, and the main conclusions are as follow.

(1) The oil film forces are very sensitive to the end seal clearance. In general, as the thickness of the end sealing clearance decreases, oil flow is obstructed within the ISFD, and internal pressure within the ISFD is increased. The tangential forces of squeeze film shows opposite trends with the decrease of end seal clearance. Damping is also very sensitive to the end seal clearance. When the end seal clearance is reduced to a half of its original size, the damping is increased by 5 times.

(2) With the increases of the vibration amplitude, the amplitude of oil film force fluctuation in  $X$  direction and  $Y$  direction increases. The damping of ISFD is almost constant under different vibration amplitude. In other words, the increase of vibration amplitude does not lead to the increase of the damping coefficient, but does lead to the instability of the oil film force.

(3) With the increases of the oil supply pressure, there are more high-pressure parts in the ISFD pressure distribution. Damping is affected by tangential forces of oil film. Damping shows an increased tendency when oil supply pressure increases due to the increase of the tangential forces.

(4) In conclusion, it is found that the necessary condition for the increase of the damping is that the oil film force needs to increase. Making the flow of oil more difficult is an effective way to increase damping.

#### References

- [ 1 ] HAMBURG G, PARKINSON J. Gas turbine shaft dynamics[J]. *SAE Transactions*, 1962, 70: 774-784
- [ 2 ] ADOLFO D, LUIS S A. Nonlinear identification of mechanical parameters in a squeeze film damper with integral mechanical seal[J]. *Journal of Engineering for Gas Turbines and Power*, 2009, 131(4): 95-101
- [ 3 ] PINKUS O, STERNLICHT B. Theory of Hydrodynamic Lubrication[M]. New York: McGraw-Hill, 1961
- [ 4 ] GEHANNIN J, ARGHIR M, BONNEAU O. Complete modeling of squeeze film dampers using the bulk flow model[C]//Proceedings of the STLE/ASME International Joint Tribology Conference American Society of Mechanical Engineers, Miami, USA, 2008:20-22
- [ 5 ] HUMES B. The Nonlinear Performance of Squeeze Film Damper[D]. Brighton: University of Sussex, 1977
- [ 6 ] MAGGE N. Philosophy, design, and evaluation of soft-mounted engine rotor systems[J]. *Journal of Aircraft*, 1975, 12(4):318-324
- [ 7 ] VANCE J M, ROYAL A C. High-speed rotor dynamics-an assessment of current technology for small turboshaft engines[J]. *Journal of Aircraft*, 1975, 12(4):295-305
- [ 8 ] MEMMOT T, EDMUND A. Stability of centrifugal compressors by applications of tilt pad seals, damper bearings, and shunt holes[C]//Proceedings of the IMechE 5th International Conference on Vibrations in Rotating Machinery, Bath, UK, 1992:7-10
- [ 9 ] PIETRA L D, DELLA L, ADILETTA G, et al. The squeeze film damper over four decades of investigations. Part I: characteristics and operating features[J]. *Shock and Vibration Digest*, 2002, 34:3-26
- [ 10 ] ADILETTA G, PIETRA L D. The squeeze film damper over four decades of investigations. Part II: rotor dynamic analyses with rigid and flexible rotors[J]. *Shock and Vibration Digest*, 2002, 34(2):97-126
- [ 11 ] SHIAU T N, WANG C R, LIU D S, et al. Nonlinear dynamic study on effects of rub-impact caused by oil-rupture in a multi-shafts turbine with a squeeze film damper[C]//ASME Turbo Expo 2014: Turbine Technical Conference and Exposition, Dusseldorf, Germany, 2014:1-10
- [ 12 ] TAYLOR D L, FEHRV S. Analysis and design of segmented dampers for rotor dynamic control[J]. *Journal of Lubrication Technology*, 1982, 104(1): 84-90
- [ 13 ] FERFECKI P, ZAPOMÉL J, GEBAUER M, et al. A computational fluid dynamics investigation of the segmented integral squeeze film damper[C]//MATEC Web of Conferences, Online, 2019: 08005
- [ 14 ] YAN W, HE L, ZHU G, et al. Experimental study on vibration suppression in a rotor system under base excitation using an integral squeeze film damper[J]. *High Technology Letters*, 2020, 26(4): 349-359
- [ 15 ] YAN W, HE L, ZHANG Y, et al. Experimental study of suppressing the unbalanced response vibration of rotor system with a G-type integral squeeze film damper[J]. *High Technology Letters*, 2021, 27(1): 1-9
- [ 16 ] LU K, HE L, ZHANG Y, et al. Experimental study on vibration suppression of gear shaft misalignment with ISFD[J]. *High Technology Letters*, 2019, 25(1):17-27
- [ 17 ] LU X, ANDRÉS L S, KOO B, et al. On the effect of the gap of end seals on force coefficients of a test integral squeeze film damper: experiments and predictions[J]. *Journal of Engineering for Gas Turbines and Power*, 2021, 143(1):011014
- [ 18 ] BUGRA E, ADOLFO D, JEFFREY M. Dynamic characterization of an integral squeeze film bearing support damper for a supercritical  $\text{CO}_2$  expander[J]. *Journal of Engineering for Gas Turbines and Power*, 2018, 140(5): 1-9

**LI Geng**, born in 1997. He is studying for his M. S. degree in Engineering Research Center of Chemical Safety Ministry of Education of Beijing University of Chemical Technology. He received his B. S. degree in Beijing University of Chemical Technology in 2019. His research interests include the vibration control and rotating machinery.